



# Binder-free highly conductive graphene laminate for low cost printed radio frequency applications

Xianjun Huang,<sup>1</sup> Ting Leng,<sup>1</sup> Xiao Zhang,<sup>1</sup> Jia Cing Chen,<sup>2</sup> Kuo Hsin Chang,<sup>2</sup> Andre K. Geim,<sup>3</sup> Kostya S. Novoselov,<sup>4</sup> and Zhirun Hu<sup>1,a)</sup>

<sup>1</sup>*School of Electrical and Electronic Engineering, University of Manchester, Manchester, United Kingdom*

<sup>2</sup>*BGT Materials Limited, Photon Science Institute, University of Manchester, Manchester M13 9PL, United Kingdom*

<sup>3</sup>*Manchester Centre for Mesoscience and Nanotechnology, University of Manchester, Manchester, United Kingdom*

<sup>4</sup>*School of Physics and Astronomy, University of Manchester, Manchester, United Kingdom*

(Received 9 March 2015; accepted 24 April 2015; published online 19 May 2015)

In this paper, we demonstrate realization of printable radio frequency identification (RFID) antenna by low temperature processing of graphene ink. The required ultra-low resistance is achieved by rolling compression of binder-free graphene laminate. With compression, the conductivity of graphene laminate is increased by more than 50 times compared to that of as-deposited one. Graphene laminate with conductivity of  $4.3 \times 10^4$  S/m and sheet resistance of  $3.8 \Omega/\text{sq}$  (with thickness of  $6 \mu\text{m}$ ) is presented. Moreover, the formation of graphene laminate from graphene ink reported here is simple and can be carried out in low temperature ( $100^\circ\text{C}$ ), significantly reducing the fabrication costs. A dipole antenna based on the highly conductive graphene laminate is further patterned and printed on a normal paper to investigate its RF properties. The performance of the graphene laminate antenna is experimentally measured. The measurement results reveal that graphene laminate antenna can provide practically acceptable return loss, gain, bandwidth, and radiation patterns, making it ideal for low cost printed RF applications, such as RFID tags and wearable wireless sensor networks. © 2015 AIP Publishing LLC. [<http://dx.doi.org/10.1063/1.4919935>]

Printed electronics is an emerging technology which grows rapidly due to its wide applications in flexible display,<sup>1,2</sup> biomedical/chemical sensor,<sup>3–5</sup> radio frequency identification (RFID),<sup>6,7</sup> wearable electronics,<sup>8</sup> energy harvesting and storage, etc.<sup>9,10</sup> As electrical conductor is the core component in printed electronics, the main research has been focused on providing high conductive inks.

Currently, conductive inks can be classified into several categories, such as metal nanoparticles,<sup>11</sup> conductive polymers,<sup>12</sup> and carbon nanomaterials,<sup>13,14</sup> to name a few. Metal nanoparticles pose high conductivity. Among them, silver nanoparticles are popular, but expensive. Copper or aluminum nanoparticles are prone to become oxidized.<sup>11,15</sup> The more challenging issue is the compatibility with other heat-sensitive electronic components as annealing treatment in high temperature is required when making patterns.<sup>14</sup> As to conductive polymer, it is economical but not conductive enough for many applications.<sup>12</sup> Conductive polymer is also limited by chemical and thermal instability.<sup>16</sup> Carbon nanomaterials, especially graphene, are quite competitive in providing high conductive ink along with advantages in cost, chemical stability, and mechanical flexibility.<sup>17,18</sup>

To integrate with printing devices, graphene inks are reported to be prepared generally in two ways. One is to disperse graphene directly in solvents like N-Methyl-2-pyrrolidone or Dimethylformamide (NMP/DMF) with no binder,<sup>18,19</sup> and the other is to use binders like ethyl cellulose (EC).<sup>17,20</sup> To date, graphene ink containing binder (EC) was reported to offer conductivity of  $2.5 \times 10^4$  S/m through reduced graphene oxide (RGO).<sup>17</sup> However, binders are

insulators and they reduce the conductivity of the inks. To increase the conductivity, thermal annealing at  $250^\circ\text{C}$  for 30 min is needed to decompose binder (EC) and reduce graphene oxide after patterning procedure.<sup>17</sup> However, thermal annealing makes it unsuitable to be applied on heat-sensitive substrates like paper, plastics, etc.<sup>14</sup> In contrary, binder-free ink reduces the requirement of annealing. For example, a typical  $70^\circ\text{C}$  treatment was implemented in preparing binder-free graphene patterns with conductivity of  $3 \times 10^3$  S/m.<sup>19</sup> While binder-free graphene ink has advantages in low temperature processing, its conductivity is low and requires further improvement.

Herein, we present a simple but effective technique to enhance the conductivity of binder-free graphene ink for industrial scale screen printing. The conductivity of graphene laminate is improved by more than 50 times with rolling compression, reaching  $4.3 \times 10^4$  S/m, almost double of  $2.5 \times 10^4$  S/m of previously reported RGO with binder<sup>17</sup> and ten times higher than that of binder-free.<sup>19</sup> To investigate the RF properties of the material, a printed graphene laminate dipole antenna on a paper substrate has been fabricated. The measurement results have demonstrated its effective radiation in all aspects of impedance matching, gain, and radiation pattern. These results reveal its valuable prospective in RFID and other printed RF applications.

In this paper, we first introduce the rolling compression method to improve the conductivity of graphene laminates, and then present printed RF antenna and its performance.

Conductive inks generally contain at least one kind of binders such as polymeric, epoxy, siloxane, and resin because granular powders cannot form a continuous film without linkages by binders. However, binders reduce the conductivity of ink as they are insulators. To maintain the

<sup>a)</sup>Author to whom correspondence should be addressed. Electronic mail: Z.Hu@manchester.ac.uk.

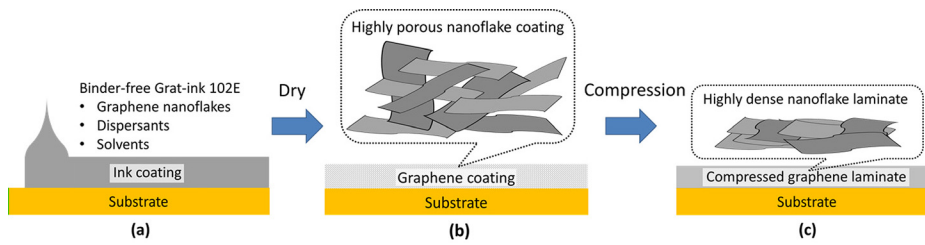


TABLE I. Resistivity and conductivity of as-deposited and various compressed graphene laminate.

Samples	1 <sup>a</sup>	2	3	4
Compression ratio (%)		70	27	19
Thickness $t$ ( $\mu\text{m}$ )	31.6	22.1	8.4	6.0
$R_s^b$ ( $\Omega/\text{sq}$ )	38.0	28.5	8.2	3.8
Normalized $R_s^c$ ( $\Omega/\text{sq}/\text{mil}$ )	48.0	25.0	2.7	0.9
Resistivity $\rho$ ( $\Omega\text{ m}$ )	$1.2 \times 10^{-3}$	$6.3 \times 10^{-4}$	$6.9 \times 10^{-5}$	$2.3 \times 10^{-5}$
Conductivity $\sigma$ ( $\text{S m}^{-1}$ )	$8.3 \times 10^2$	$1.6 \times 10^3$	$1.4 \times 10^4$	$4.3 \times 10^4$

<sup>a</sup>Sample 1 is as-deposited, namely, no compression.

<sup>b</sup>Sheet resistance of samples.

<sup>c</sup>Normalize sheet resistance 1 mil.

ink conductivity, the amount of conductive solids needs to be increased when insulation binders are used. Here, we proposed a strategy to prepare a graphene laminate of high conductivity without any kind of binders.

The formation of the highly conductive graphene laminate is illustrated in Fig. 1. In this work, binder-free graphene ink (Grat-ink 102E, BGT Materials Limited) was used. The ink in Fig. 1(a) contains graphene nanoflakes, dispersants, and solvents, but no binders were used in the recipe of graphene ink. It is known that free-standing graphene films were robust and flexible, and such excellent film-forming ability of graphene is unique from other conductive materials.<sup>21</sup> After drying, the adhesion of graphene coating comes from the good film-forming ability of graphene nanoflakes, resulting from its 2D structure. However, the contact resistance between graphene nanoflakes is high in the as-deposited graphene coating because the stacking of graphene nanoflakes is highly porous, as illustrated in Fig. 1(b). So further rolling compression is applied to enhance the conductivity and improve the adhesion of graphene laminate. After compression, the graphene nanoflakes become highly dense and graphene laminate forms, as shown in Fig. 1(c).

To study the effects of the rolling compression, four kinds of samples with various compression ratios were

FIG. 1. Schematic illustration of binder-free graphene laminate formation. No binder was used in graphene ink due to the strong Van der Waals' force of graphene nanoflakes. The adhesion and conductivity of graphene laminate were further improved by rolling compression.

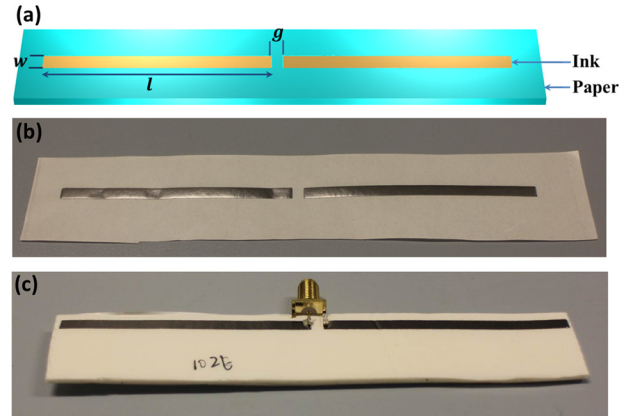


FIG. 3. (a) Geometric dimension of the dipole antenna, (b) photo of the printed graphene laminate dipole antenna, and (c) graphene laminate antenna connected with a SMA for measurement.

prepared and measured. The compression ratio is the thickness ratio of compressed samples over as-deposited samples. The sheet resistance of these graphene laminates was measured by the 4-point probe (RM3000, Jandel). The thicknesses of as-deposited and compressed graphene laminate patterns were obtained by digital thickness gauge (PC-485, Teclock). A total of 10 measurements at different spots were carried out to obtain the average value of each sample. With measured thickness and sheet resistance, the normalized sheet resistance to 1 mil (equal to  $25.4 \mu\text{m}$ ), resistivity, and bulk conductivity are calculated and summarized in Table I.

As it can be seen from Table I, the normalized sheet resistance of as-deposited graphene laminate was  $48.0 \Omega/\text{sq}/\text{mil}$  (sample 1), which can be significantly reduced by 53 times to  $0.9 \Omega/\text{sq}/\text{mil}$  (sample 4) after 19% compression. The effect of rolling compression on laminate morphology was further studied by the SEM observation, as displayed in Fig. 2. The surface of as-deposited graphene laminate exhibits a porous and irregular architecture (see Fig. 2(a)), which results in a high contact resistance and unsmooth pathways for electron transport. After rolling compression (19% compression

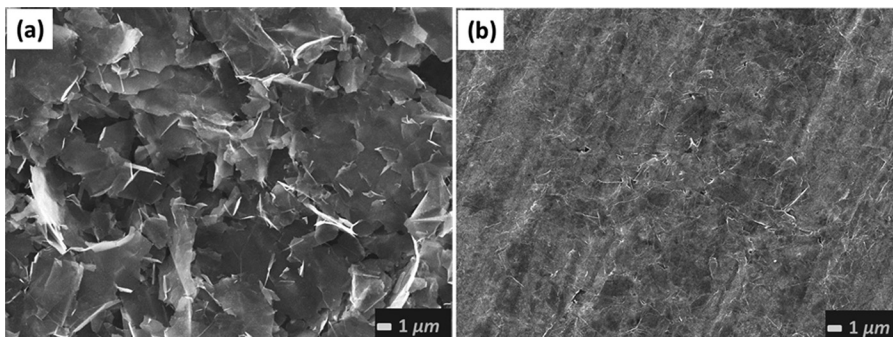


FIG. 2. SEM images of (a) as-deposited and (b) compressed graphene laminates.



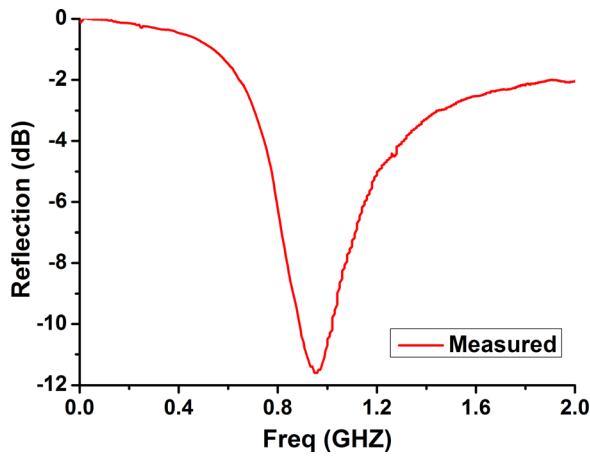


FIG. 4. Measured reflection of graphene laminate dipole antenna.

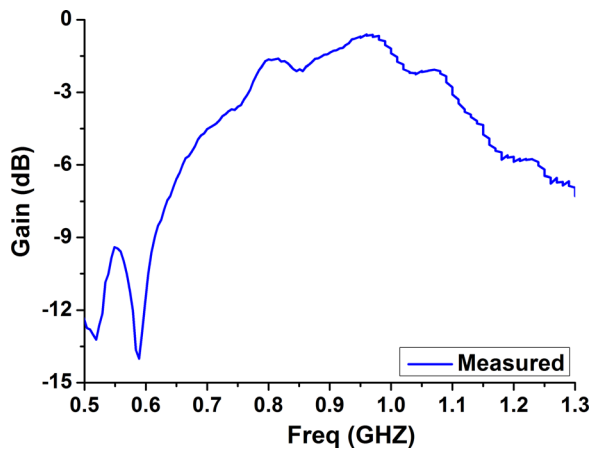


FIG. 5. Measured realized gain of graphene laminate dipole antenna.

ratio), dense and continuous graphene laminate is obtained (see Fig. 2(b)). Therefore, the compressed graphene laminate exhibits much lower sheet resistances in comparison to as-deposited sample.

From the above analysis, it should be noticed that not only the conductivity increases significantly with compression but also the sheet resistance of graphene laminate reduces to  $3.8 \Omega/\text{sq}$  from  $38 \Omega/\text{sq}$ . In antenna applications, especially in RF band, sheet resistance matters more. In the previous work, a graphene printed antenna with sheet resistance of  $65 \Omega/\text{sq}$  was proved to be well matched, while no effective radiation was demonstrated.<sup>9</sup>

To investigate RF radiation properties of the binder-free graphene laminate, a half-wavelength dipole antenna was

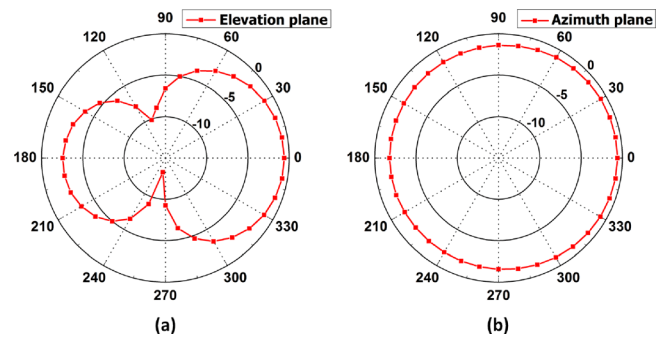


FIG. 7. Measured gain radiation patterns. (a) Elevation plane and (b) Azimuth plane.

designed. A normal paper was used as a substrate for possible flexible applications. Similar with the process shown in Fig. 1, antenna patterns were first printed by 150 mesh stainless-steel screen and then dried at  $100^\circ\text{C}$  for 10 min. A compression roller (SERP02, Shining Energy) was further used to obtain compressed samples. With 4-point probe test (RM3000, Jandel), the sheet resistance of the graphene laminate antenna pattern was measured to be  $3 \Omega/\text{sq}$ . The final thickness after compression was  $7.7 \mu\text{m}$ , measured with digital thickness gauge (PC-485, Teclock).

In the fabrication, no high temperature thermal annealing or vacuum condition is required. This not only makes printing compatible with paper/plastics but also lowers the costs of manufacturing significantly. Moreover, the screen printing is ideal for high-throughput and low-cost mass commercial production.

The dipole antenna made of binder-free graphene laminate was printed on paper, as shown in Fig. 3. The length of one arm is  $l = 68.82 \text{ mm}$ , and the width and gap distance are  $w = 3.53 \text{ mm}$  and  $g = 3.53 \text{ mm}$ , respectively. The substrate paper has dielectric constant of 2.3 and is of  $50 \mu\text{m}$  thickness.

Due to the flexibility of graphene laminate, the antenna is flexible when printed on paper or plastic, which is quite important for flexible electronics like wearable and RFID applications. To facilitate the test, a thin foam layer (RS 554-844) with thickness of 0.8 mm and dielectric constant of 2.6 is laid under the paper for support. A SMA (SubMiniature version A) connector is connected with graphene laminate antenna with conductive epoxy (Circuit works CW2400), as shown in Fig. 3(c).

The reflection coefficient ( $S_{11}$ ) of the graphene laminate antenna was measured with Vector Network Analyzer (VNA Agilent E5071B) and is shown in Fig. 4. As it can be seen, the minimum reflection occurs at 960 MHz with  $-11.6 \text{ dB}$ ,

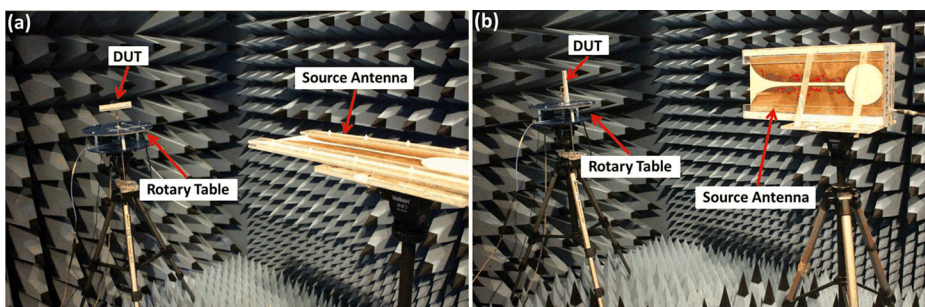


FIG. 6. Radiation pattern measurement in anechoic chamber. (a) Elevation plane measurement; and (b) Azimuth plane measurement.

indicating that the antenna is well matched. The  $-10$  dB bandwidth is from 0.89 GHz to 1.02 GHz, which means that above 90% power is transmitted to the antenna in this band.

However, good impedance matching, i.e., low reflection coefficient ( $S_{11}$ ), only indicates that power is effectively transmitted from the source to the antenna. It does not tell if the transmitted power is effectively radiated to the free space. The transmitted power from the source can be partly dissipated due to the ohmic loss of the antenna.<sup>22,23</sup> The higher the sheet resistance is, the less the RF power will be radiated. As one of the most important criteria of antenna performance evaluation, the realized gain is necessary to show the effectiveness of radiation. In this work, the realized gain of the graphene laminate antenna was tested with three antenna method.<sup>24</sup> As displayed in Fig. 5, the realized gain peaks to  $-0.6$  dBi at 962 MHz, and between 930 MHz and 990 MHz, the gain is above  $-1$  dBi. Although it is well known that the realized gain of an ideal half-wavelength dipole antenna is 2.14 dBi in theory, the gain achieved here is good enough for many wearable and RFID applications. Take RFID chip Ucode 7 (NXP Semiconductors) as an example, provided the impedance matching between chips and antenna is satisfied, the maximum reading range can exceed 10 m with antenna of  $-1$  dBi gain.

To further verify the radiation, the radiation pattern at 962 MHz was measured in our anechoic chamber as shown in Fig. 6. Vivaldi antenna is used as radiator and DUT (Device Under Test, graphene laminate antenna) is placed on a rotary table as receiver. These two antennas are connected with VNA (Agilent E5071B, USA), and radiation pattern is recorded with antenna measurement system (Antenna Measurement Studio 5.5, Diamond Engineering). The data were recorded for every  $10^\circ$  rotation. Combining with the gain value at 962 MHz, the radiation pattern is displayed in Fig. 7.

As it can be seen in Fig. 7, the radiation pattern shows a typical dipole pattern. In Fig. 7(a), a bit smaller radiation on the left side radiation is due to the influence of pasted foam layer. At  $0^\circ$ , the gain is maximum ( $-0.6$  dBi). When it rotates to around  $90^\circ$  and  $270^\circ$ , the gain becomes the lowest. Azimuth plane radiation is a typical circle, which is expected for a dipole antenna. The radiation pattern again proves that

the printed graphene laminate dipole antenna can radiate effectively.

In conclusion, rolling compression method was demonstrated to be effective in significantly improving the conductivity of binder-free graphene laminate. A printed graphene laminate dipole antenna has been experimentally verified to radiate RF power effectively, which demonstrates the feasibility of graphene laminate for printed RF applications.

<sup>1</sup>V. Wood, M. J. Panzer, J. Chen, and V. Bulović, *Adv. Mater.* **21**, 2151 (2009).

<sup>2</sup>S. Azouel, S. Shemesh, and S. Magdassi, *Nanotechnology* **23**, 344003 (2012).

<sup>3</sup>J. Jang, J. Ha, and J. Cho, *Adv. Mater.* **19**, 1772 (2007).

<sup>4</sup>L. Huang, Y. Huang, J. Liang, X. Wan, and Y. Chen, *Nano Res.* **4**, 675 (2011).

<sup>5</sup>V. Dua, S. P. Surwade, S. Ammu, S. R. Agnihotra, S. Jain, K. E. Roberts, and S. K. Manohar, *Angew. Chem., Int. Ed.* **49**, 2154 (2010).

<sup>6</sup>S. Magdassi, M. Grouchko, and A. Kamysny, *Materials* **3**, 4626 (2010).

<sup>7</sup>K. Y. Shin, J. Y. Hong, and J. Jang, *Adv. Mater.* **23**, 2113 (2011).

<sup>8</sup>B. Schmied, J. Günther, C. Klatt, H. Kober, and E. Raemaekers, *Adv. Sci. Technol.* **60**, 67 (2009).

<sup>9</sup>A. M. Gaikwad, G. L. Whiting, D. A. Steingart, and A. C. Arias, *Adv. Mater.* **23**, 3251 (2011).

<sup>10</sup>C. N. Hoth, S. A. Choulis, P. Schilinsky, and C. J. Brabec, *Adv. Mater.* **19**, 3973 (2007).

<sup>11</sup>H. H. Lee, K. S. Chou, and K. C. Huang, *Nanotechnology* **16**, 2436 (2005).

<sup>12</sup>A. G. Del Mauro, R. Diana, I. A. Grimaldi, F. Loffredo, P. Morvillo, F. Villani, and C. Minarini, *Polym. Compos.* **34**, 1493 (2013).

<sup>13</sup>W. R. Small and M. I. H. Panhuis, *Small* **3**, 1500 (2007).

<sup>14</sup>A. Kamysny and S. Magdassi, *Small* **10**, 3515 (2014).

<sup>15</sup>T. J. Foley, C. E. Johnson, and K. T. Higa, *Chem. Mater.* **17**, 4086 (2005).

<sup>16</sup>S. M. Richardson-Burns, J. L. Hendricks, B. Foster, L. K. Povlich, D. H. Kim, and D. C. Martin, *Biomaterials* **28**, 1539 (2007).

<sup>17</sup>E. B. Secor, P. L. Prabhurashi, K. Puntambekar, M. L. Geier, and M. C. Hersam, *J. Phys. Chem. Lett.* **4**, 1347 (2013).

<sup>18</sup>F. Torrisi, T. Hasan, W. Wu, Z. Sun, A. Lombardo, T. S. Kulmala, and A. C. Ferrari, *ACS Nano* **6**, 2992 (2012).

<sup>19</sup>D. J. Finn, M. Lotya, G. Cunningham, R. J. Smith, D. McCloskey, J. F. Donegan, and J. N. Coleman, *J. Mater. Chem. C* **2**, 925 (2014).

<sup>20</sup>J. Li, F. Ye, S. Vaziri, M. Muhammed, M. C. Lemme, and M. Östling, *Adv. Mater.* **25**, 3985 (2013).

<sup>21</sup>M. Lotya, P. J. King, U. Khan, S. De, and J. N. Coleman, *ACS Nano* **4**, 3155 (2010).

<sup>22</sup>J. S. Gomez-Diaz and J. Perruisseau-Carrier, in *Proceedings of the IEEE International Symposium on Antennas and Propagation (ISAP)*, Nagoya, Japan, 29 October 2012–02 November 2012, pp. 239–242.

<sup>23</sup>C. A. Balanis, *Antenna Theory: Analysis and Design* (John Wiley & Sons, Hoboken, 2012), pp. 60–62.

<sup>24</sup>C. A. Balanis, *Antenna Theory: Analysis and Design* (John Wiley & Sons, Hoboken, 2012), pp. 867–868.